Hadro-quarkonium from Lattice QCD

Maurizio Alberti, Gunnar S. Bali, Sara Collins, Francesco Knechtli, Graham Moir, and Wolfgang Söldner

¹Department of Physics, Bergische Universität Wuppertal, Gauβstraβe 20, 42119 Wuppertal, Germany

²Institut für Theoretische Physik, Universität Regensburg,

Universitätsstraβe 31, 93053 Regensburg, Germany

³ Department of Theoretical Physics, Tata Institute of Fundamental Research, Homi Bhabha Road, Mumbai 400005, India ⁴ Department of Applied Mathematics and Theoretical Physics, Centre for Mathematical Sciences, University of Cambridge, Wilberforce Road, Cambridge, CB3 0WA, UK

The hadro-quarkonium picture [S. Dubinskiy and M.B. Voloshin, Phys. Lett. B **666**, 344 (2008)] provides one possible interpretation for the pentaquark candidates with hidden charm, recently reported by the LHCb Collaboration, as well as for some of the charmonium-like "X, Y, Z" states. In this picture, a heavy quarkonium core resides within a light hadron giving rise to four- or five-quark/antiquark bound states. We test this scenario in the heavy quark limit by investigating the modification of the potential between a static quark-antiquark pair induced by the presence of a hadron. Our lattice QCD simulations are performed on a Coordinated Lattice Simulations (CLS) ensemble with $N_f = 2 + 1$ flavours of non-perturbatively improved Wilson quarks at a pion mass of about 223 MeV and a lattice spacing of about $a = 0.0854 \, \mathrm{fm}$. We study the static potential in the presence of a variety of light mesons as well as of octet and decuplet baryons. In all these cases, the resulting configurations are favoured energetically. The associated binding energies between the quarkonium in the heavy quark limit and the light hadron are found to be smaller than a few MeV, similar in strength to deuterium binding. It needs to be seen if the small attraction survives in the infinite volume limit and supports bound states or resonances.

I. INTRODUCTION

Recently, the LHCb Collaboration found two structures in the decay $\Lambda_b \to J/\psi p K$, which can be interpreted as candidates for pentaguark states with hidden charm, containing three light quarks, in addition to a charm quark-antiquark pair [1, 2]. The most likely spin and parity assignments for these candidates, labelled $P_c^+(4380)$ and $P_c^+(4450)$, are $J^P = 3/2^-$ and $5/2^+$, respectively, with $3/2^+$ and $5/2^-$ being another possibility. While the nature of these (and of some other structures) is still disputed [3, 4], the number of established charmonium resonances certainly has exploded during the past 15 years, see Ref. [5] and, e.g., Ref. [6] for a more recent review. Many of these are of an exotic nature and some clearly hint at light quark-antiquark or — in the case of the P_c candidates — even at qqq components, in addition to the charm quark and antiquark.

Many models can accommodate some, or if extended to include states that contain five (anti-)quarks, even all of these resonances: tetraquarks [7–9] consisting of diquark-antidiquark pairs, including a recently proposed "dynamic" picture [10, 11], molecules of two open charm mesons [12–16], hybrid states [17–20] containing a charm quark-antiquark pair and additional valence gluons, hadro-charmonium with a compact charmonium core bound inside a light hadron [21, 22], and mixtures of the above. Here we will specifically aim to establish if the last picture (hadro-quarkonium) is supported in the heavy quark limit.

The standard way of addressing a strongly decaying resonance and extracting the position of the associated pole in the unphysical Riemann sheet from simulations in Euclidean spacetime boxes was introduced by

Lüscher [23]. For applications of this and related methods to charmonium spectroscopy, see, e.g., Ref. [24] and references therein. In the case of charmonia, this is particularly challenging since, in addition to ground states, radial excitations need to be considered and the number of different decay channels can be large, some with more than two hadrons in the final state. Moreover, while in principle resonance parameters can be computed, at least below inelastic multi-particle thresholds, these will not necessarily tell us much about the "nature" of the underlying state: how does the naive quark model need to be modified to provide a guiding principle for the existence or non-existence of an exotic resonance?

A direct computation of the scattering parameters of, e.g., a nucleon-charmonium resonance in a realistic setting constitutes a serious computational challenge, especially if one aims at conclusive results with meaningful errors. Instead of directly approaching the problem at hand, here we restrict ourselves to the heavy quark limit in which the charm quarks can be considered as slowly moving in the background of gluons, sea quarks and, possibly, light hadrons.

After integrating out the degrees of freedom associated with the heavy quark mass m_Q , quarkonia can be described in terms of an effective field theory: non-relativistic QCD (NRQCD) [25]. In the limit of small distances r, or equivalently, large momentum transfers $m_Q v$, where v is the interquark velocity, the scale $m_Q v \sim 1/r$ can also be integrated out, resulting in potential NRQCD (pNRQCD) [26, 27]. Then, to leading order in r with respect to the pNRQCD multipole expansion and to $v^2 \sim \alpha_s$ in the NRQCD power counting, quarkonium becomes equivalent to a non-relativistic quantum mechanical system, where the interaction potential is given by

the static potential $V_0(r)$ which can, e.g., be computed non-perturbatively from Wilson loop expectation values $\langle W(r,t) \rangle$ in Euclidean spacetime:

$$V_0(r) = -\lim_{t \to \infty} \frac{\mathrm{d}}{\mathrm{d}t} \ln \langle W(r, t) \rangle. \tag{1}$$

Here we investigate whether this potential becomes modified in the presence of a light hadron. This would then lower or increase quarkonium energy levels. If embedding the quarkonium in the light hadron is energetically favourable, this would suggest a bound state, at least for sufficiently large quark masses.

This article is organized as follows. In Sec. II we briefly discuss previous studies of nucleon-charmonium bound states and comment on the ordering of scales that we consider. In Sec. III we define the observables that we compute. Then, in Sec. IV we describe details of the simulation, before numerical results are presented in Sec. V. Subsequently, in Sec. VI we relate the modifications of the static potential to quarkonium bound state energies, before we summarize in Sec. VII.

II. NUCLEON-CHARMONIUM BOUND STATES

Light meson exchanges between a single nucleon or nucleons bound in a nucleus and quarkonium, which does not contain any light valence quarks, are suppressed by the Zweig rule. Therefore, such interactions should be dominated by gluon exchanges. In the heavy quark limit, quarkonium can be considered essentially as a point particle of a heavy quark and antiquark bound by the short-range perturbative Coulomb potential. The first non-vanishing chromodynamical multipole is then a dipole and quarkonium may interact with the nuclear environment via colour dipole-dipole van der Waals forces. For a recent discussion of the relevant scales in the context of effective field theories, see Ref. [28]. Initially, using phenomenological interaction potentials, nucleon-charmonium binding energies ranging from 20 MeV [29, 30] down to 10 MeV [31] were estimated for nuclei consisting of A > 3 [29, 31] and A > 10 [30] nucleons. A first QCD based estimate [32] for the potential between quarkonium in the heavy quark limit and a nucleus resulted in Υ and J/ψ binding energies of a few MeV and 10 MeV, respectively, possibly with large relativistic and higher order multipole corrections in the charmonium case. This discussion of light nuclei hosting a quarkonium state may have contributed to the suggestion of quarkonium states that are embedded within light hadrons, hadro-quarkonia [21].

At present no (p)NRQCD lattice studies of baryoncharmonium states exist. However, a few investigations employing relativistic charm quarks have been carried out. In Ref. [33], the η_c and J/ψ charmonia were scattered with light pseudoscalar and vector mesons as well as with the nucleon, in the quenched approximation with rather large light quark mass values; the ratio M_{π}/m_{ρ} ranged from 0.9 down to 0.68. Varying the lattice extent from $L = 1.6 \,\mathrm{fm}$ over $2.2 \,\mathrm{fm}$ up to $3.2 \,\mathrm{fm}$, in this pioneering work scattering lengths were extracted, indicating some attraction in all the channels investigated. A similar study was performed in Ref. [34], combining staggered sea with domain wall light and Fermilab charm quarks, however, unusually small scattering lengths were reported. Finally, a pseudoscalar charm quark-antiquark pair was created along with a nucleon and even with light nuclei by the NPLQCD Collaboration [35]. In this work the binding energy reported for the nucleon case was about 20 MeV, albeit at a rather large light quark mass value, corresponding to $M_{\pi} \approx 800 \,\mathrm{MeV}$, and for a coarse lattice spacing $a \approx 0.145 \,\mathrm{fm}$. This value of the binding energy is consistent with some of the expectations for charmonia in a nuclear environment discussed above.

Closest in spirit to the van der Waals interaction picture, Kawanai and Sasaki [36] in a quenched study, again at rather large pion masses, $M_{\pi} \geq 640 \,\mathrm{MeV}$, computed a charmonium-nucleon Bethe–Salpeter wave function. Plugging this into a Schrödinger equation, a potential between the charmonium and the nucleon was extracted, indicating very weak attractive forces.

Here we will not assume a non-relativistic light hadron of mass m_H , whose dipole-dipole interaction with quarkonium can be described by a potential. Instead, our light hadron is an extended relativistic object. We also go beyond the point-dipole approximation in the heavy quark sector by "pulling" quark and antiquark apart by a distance r. We then determine the modification of the interaction potential between the heavy quark-antiquark pair, that we approximate as static sources, induced by the presence of a light hadron. To be more precise, we will consider the limit $m_Q \gg m_H$, $m_Q \gg \Lambda_{\rm QCD}$, where $\Lambda_{\rm QCD}$ denotes a typical non-perturbative scale of a few hundred MeV, and $v^2 \ll 1$. Since we determine the quarkantiquark potential, i.e. the matching function between NRQCD and pNRQCD, nonperturbatively, $m_Q v \sim 1/r$ does not need to be much larger than $\Lambda_{\rm QCD}$. However, we neglect colour octet contributions [26, 27], which may become significant at distances $r \gtrsim \Lambda_{\rm QCD}^{-1}$.

III. STATIC POTENTIALS "INSIDE" HADRONS

We denote an interpolator creating a static fundamental colour charge Q at a position $\mathbf{z} + \mathbf{r}/2$ and destroying it at a position $\mathbf{z} - \mathbf{r}/2$ as $Q_{\mathbf{r}}^{\dagger}(\mathbf{z})$. This will transform according to the fundamental $\mathbf{3}$ representation of the gauge group at $\mathbf{z} + \mathbf{r}/2$ and according to $\mathbf{3}^*$ at $\mathbf{z} - \mathbf{r}/2$ and hence it contains a gauge covariant transporter connecting these two points (usually a spatially smeared Schwinger line). The Wilson loop can then be written as

$$\langle W(r,t)\rangle = \langle 0|\mathcal{Q}_r \mathcal{T}^{t/a} \mathcal{Q}_r^{\dagger}|0\rangle, \qquad (2)$$

where we assume rotational invariance is restored for $r = |\mathbf{r}| \gg a$, and $\mathcal{T} = e^{-a\mathbb{H}}$ denotes the transfer matrix connecting adjacent time slices.

Within the static approximation, there are different strategies to investigate bound states containing a heavy quark-antiquark pair and additional light quarks. One method, which we are not going to pursue here, amounts to creating a light hadron H containing either $\bar{q}q$ or qqq along with the stringy $Q\bar{Q}$ state at equal Euclidean time. The interpolator for creating a zero momentum projected tetra- or pentaquark state then has the form

$$\overline{\mathcal{P}}_r = \sum_{\mathbf{z}} \overline{\mathcal{H}}(\mathbf{z}) \mathcal{Q}_r^{\dagger}(\mathbf{z}). \tag{3}$$

Note that the creation interpolator $\overline{\mathcal{H}}$ of a hadronic state (as well as $\overline{\mathcal{P}}_r$) will carry a spinor index, which we suppress. The correlator of interest is now $\langle 0|\mathcal{P}_r\mathcal{T}^{t/a}\overline{\mathcal{P}}_r|0\rangle$. Even without summing over positions \mathbf{z} this is automatically projected onto zero momentum at source and sink as the light hadron is tied in position space to the static quarks, see Eq. (3). Numerous possibilities exist for where to spatially place the light quarks relative to the heavy sources within the interpolator \mathcal{P}_r and how to transport and contract the colour such that the interpolator respects the correct gauge transformation properties. This freedom can be exploited to enhance the overlap of $\overline{\mathcal{P}}_r|0\rangle$ with the physical state and may also provide some insight into its internal structure.

Subsequent to a pioneering lattice study [37] of a light qq pair bound in the above way to two static anti-triplet sources, quite a few simulations of a light $q\bar{q}$ pair bound to the string state created by \mathcal{Q}_r^{\dagger} have also been carried out. Such results exist both for a light quark-antiquark pair with isospin I=1 [38–41] and I=0 [39, 42]. In contrast, a static quark-antiquark pair accompanied by three light quarks has not been investigated on the lattice so far.

Instead of creating tetra- or pentaquark states containing a heavy or static quark and the corresponding antiquark, here we wish to "directly" address a particular picture of such bound states, hadro-quarkonium [21, 22]. This will be achieved by computing differences between the static potential in the presence of a light hadron, relative to the static potential in the vacuum. The former can be obtained from the large Euclidean time decay of

$$\langle H|\mathcal{Q}_r\mathcal{T}^{t/a}\mathcal{Q}_r^{\dagger}|H\rangle$$
, (4)

where $|H\rangle$ is the ground state that is destroyed by the zero momentum interpolator

$$\mathcal{H} \equiv \sum_{\mathbf{x}} \mathcal{H}(\mathbf{x}) \,. \tag{5}$$

In order to evaluate the expectation value Eq. (4) we create a hadronic state at time 0. We then let it propagate to δt to achieve ground state dominance. At this time we create an additional quark-antiquark string by

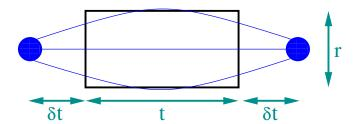


FIG. 1. Graphical representation of the four-point correlation function in the numerator of Eq. (6) for the example of a static quark-antiquark pair at a distance r embedded in a baryon. Thin blue lines correspond to light quark propagators and the black rectangle to the Wilson loop.

inserting a (smeared) Wilson loop of time extent t, which terminates at $t + \delta t$. Finally, we destroy the light hadron at the time $t + 2\delta t$. Then

$$\langle H|\mathcal{Q}_r \mathcal{T}^{t/a} \mathcal{Q}_r^{\dagger} | H \rangle$$

$$\propto \lim_{\delta t \to \infty} \frac{\langle 0|\mathcal{H} \mathcal{T}^{\delta t/a} \mathcal{Q}_r \mathcal{T}^{t/a} \mathcal{Q}_r^{\dagger} \mathcal{T}^{\delta t/a} \overline{\mathcal{H}} | 0 \rangle}{\langle 0|\mathcal{H} \mathcal{T}^{(t+2\delta t)/a} \overline{\mathcal{H}} | 0 \rangle}, \qquad (6)$$

where we average over all spatial Wilson loop positions **z** and light hadronic sink positions **x**. Zero momentum projection at the light hadronic source can be avoided, due to the translational invariance of expectation values. The correlator of interest is depicted in Fig. 1.

We can now define the potential in the background of the hadron as

$$V_H(r) = -\lim_{t \to \infty} \frac{\mathrm{d}}{\mathrm{d}t} \ln \langle H | \mathcal{Q}_r \mathcal{T}^{t/a} \mathcal{Q}_r^{\dagger} | H \rangle, \qquad (7)$$

in analogy to Eqs. (1) and (2). In the end we will compute differences

$$\Delta V_{H}(r) = V_{H}(r) - V_{0}(r)
= -\lim_{t \to \infty} \frac{\mathrm{d}}{\mathrm{d}t} \ln \frac{\langle H | \mathcal{Q}_{r} \mathcal{T}^{t/a} \mathcal{Q}_{r}^{\dagger} | H \rangle}{\langle 0 | \mathcal{Q}_{r} \mathcal{T}^{t/a} \mathcal{Q}_{r}^{\dagger} | 0 \rangle}
= -\lim_{t \to \infty} \frac{\mathrm{d}}{\mathrm{d}t} \ln \frac{\langle W(r, t) C_{H,2\mathrm{pt}}(t + 2\delta t) \rangle}{\langle W(r, t) \rangle \langle C_{H,2\mathrm{pt}}(t + 2\delta t) \rangle}, \quad (8)$$

where the argument of the logarithm is simply the correlator of a light hadronic two-point function with the Wilson loop inserted, divided by the Wilson loop expectation value times the hadronic two-point function $\langle C_{H,2pt}(t+2\delta t)\rangle = \langle 0|\mathcal{H}\mathcal{T}^{(t+2\delta t)/a}\overline{\mathcal{H}}|0\rangle$, see the denominator of Eq. (6).

We are now in the position to address the question within what hadronic channels $\Delta V_H(r)$ will be attractive and in what cases repulsive. This may serve as an indicator for the stability of related hadro-quarkonia. In view of the recent LHCb result [1, 2] baryonic states $|H\rangle$ are particularly interesting. For instance, adding the mass of the Δ to that of the J/ψ gives 4329 MeV [43], which is not far away from the mass of the $P_c(4380)$. Furthermore, $J^P=3/2^+$ can couple to 1^- to give $3/2^-$. Another

example is the sum of the nucleon (N) and χ_{c2} masses, 4496 MeV, which is close to the mass of the P_c^+ (4450). Again, $1/2^+$ and 2^+ can couple to $J^P = 5/2^+$.

IV. IMPLEMENTATION AND TECHNICAL DETAILS

We analyse the $N_f = 2+1$ ensemble "C101", which has a volume of 96×48^3 sites and was generated by the Coordinated Lattice Simulations (CLS) effort [44] using the OPENQCD simulation program [45, 46]. Open boundary conditions in time and non-perturbatively ordera improved Wilson Fermions on top of the tree level Symanzik improved Wilson gauge action are employed, see Ref. [44] for details on the simulation. To determine the lattice spacing we extrapolate the scale parameter t_0 [47] to the physical point, where we obtain $\sqrt{8t_0}/a = 4.852(7)$ [48]. Using the continuum limit result $\sqrt{8t_0} = 0.4144(59)(37) \,\text{fm}$ [49], gives $a = 0.0854(15) \,\text{fm}$. The pion and kaon masses on this ensemble are $M_{\pi} \approx$ $223\,\mathrm{MeV}$ and $M_K \approx 476\,\mathrm{MeV}$, respectively. Note that while the pion is heavier than in nature the kaon is somewhat lighter since the sum of quark masses $2m_{\ell} + m_s$ $(m_{\ell} = m_{\nu} = m_{d})$ was adjusted to a value close to the physical one and kept constant within the main set of CLS simulations [44]. The spatial lattice extent reads $L \approx 4.6/M_{\pi} \approx 4.1 \, \text{fm}$. For details see Ref. [48].

We analyse 1552 configurations, separated by four molecular dynamic units. On each of these configurations we place hadronic sources on 12 different time slices $(30, 43, 44, \ldots, 52, 53, 65)$ at random spatial positions to reduce autocorrelations. Due to the use of open boundary conditions, we have to discard the boundary regions from our analysis. After carefully checking for translational invariance in time, we use forward and backward propagating hadronic two-point functions for the 11¹ sources placed in the central region of the lattice but propagate only forward from $t_0/a = 30$ and backward from $(t - t_0)/a = 65$. This gives a total of 24×1552 two-point functions for each light hadron and spin polarization considered. Since δt needs to be kept small to obtain statistically meaningful results, the quark propagators entering these two-point functions are Wuppertal smeared at source and sink, using spatially smeared gauge transporters, to improve the overlap with the physical ground states.

We measure the Wilson loops using the publicly available WLOOP package [50], following the method described in Ref. [51]. In a first step, all gauge links are smeared using a single iteration of hypercubic (HYP) blocking [52]. Smearing the temporal links corresponds to a particular discretization choice of the static action and results in an exponential improvement of the signal-to-noise ratio of

correlators involving static quarks [53]; HYP links reduce the coefficient of the divergent contribution to the self-energy of a static quark [39, 54–56]. In a second step we construct a variational basis of Wilson loops using four different levels (0,5,7,12) of HYP smearing restricted to the three space dimensions.

To enable the construction of the correlators Eq. (8), we separately average the Wilson loops for each direction of \mathbf{r} , pointing along one of the three spatial lattice axes, and for different temporal positions. As detailed above, due to the use of open boundary conditions, our hadronic two-point functions $C_{H,2pt}(t)$ are confined to the central time region of the lattice. We checked that ratios of Wilson loop expectation values, averaged over different temporal domains, centred about the middle of the lattice, were statistically consistent with 1. Furthermore, Eq. (8) was evaluated in two ways, restricting the Wilson loop average in the denominator to the same time slices as the averaging performed within the numerator as well as averaging the Wilson loop expectation value in the denominator within the whole region where boundary effects were negligible, from time slice 24 to 72. The two results obtained for each quantity were statistically compatible with each other and below we will make use of the larger averaging region as this resulted in slightly smaller statistical errors.

For the error analysis, we apply the standard method of Ref. [57]. We include the reweighting factors due to twisted-mass reweighting and the rational approximation for the strange quark, see Ref. [46]. We checked that carrying out a more conservative analysis, estimating the effect of slow modes [58], only affects the errors in very few cases and never by more than 30%.

The distance \mathbf{r} between the static sources breaks the continuum O(3) symmetry down to the cylindrical subgroup $O(2) \otimes \mathbb{Z}_2 = D_{\infty h}$. Regarding Fermionic representations, i.e. for baryons, the double cover is reduced accordingly. In our implementation the static sourceantisource distance \mathbf{r} is kept parallel to lattice axes. This means that the 48 element octahedral crystallographic group with reflections O_h is reduced to its 16 element subgroup D_{4h} (and its double cover O'_h to $Dih_4 \otimes Dih_1$). Therefore, when correlating hadrons with a continuum spin assignment $J \geq 1$ with the string state in the Σ_q^+ irreducible representation (irrep) of $D_{\infty h}$ (A_{1g} of D_{4h} on the lattice), care has to be taken to construct the adequate irrep of the cylindrical group. Below we address the continuum situation but we have checked that the same arguments hold regarding the lattice irreps that we use. In the case of vector mesons, for example the ϕ meson, the 1⁻ O(3) irrep will split into Π_u and Σ_u^+ , the latter also appearing in the pseudoscalar channel. To block out this undesired contribution, we need to correlate a Wilson loop with \mathbf{r} pointing in the z direction with the vector state destroyed by a polarized interpolator $(\phi_x + i\phi_y)/\sqrt{2}$. We average over cyclic permutations of x, y and z. The decuplet baryon interpolator we use, for example for the Δ baryon, gives a state maximally

¹ On time slice 47 two different spatial source positions were used.

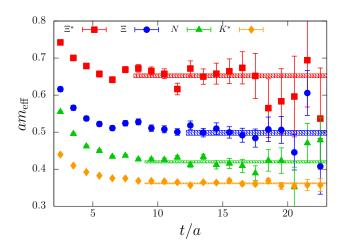


FIG. 2. Effective masses Eq. (9), extracted from various hadronic two-point functions, together with results from one-exponential fits (shaded regions).

polarized in the z direction. This then has to be correlated with a Wilson loop pointing in the z direction too, to guarantee $\Lambda = |J_z| = 3/2$ and to avoid mixing with spin 1/2 baryonic states. In this case we only used one polarization and therefore we cannot exploit averaging over different directions.

V. NUMERICAL RESULTS

Our strategy for testing the hadro-quarkonium picture is to determine the potential between two static quarks in the vacuum and to compare this with its counterpart in the presence of a hadron. An energetically favourable difference may signal a tendency of the system to bind. In Sec. V A we discuss the quality of our light hadronic effective masses and in Sec. V B we determine the potential in the vacuum, before moving on to Sec. V C, where we investigate the modifications induced by the presence of hadrons. We delay the discussion of the phenomenological consequences to Sec. VI.

A. Light hadronic effective masses

In the determination of $\Delta V_H(r)$ below we will quote the $\delta t = \delta t_{\rm opt} = 5a \approx 0.43\,{\rm fm}$ estimates as our final results. With this δt value, the fit in t to the right hand side of Eq. (8) is dominated by data with $t \leq t_{\rm max} = 10a$. Therefore, the hadronic effective masses

$$m_{H,\text{eff}}(t+a/2) \equiv a^{-1} \ln \frac{C_{H,2\text{pt}}(t)}{C_{H,2\text{pt}}(t+a)}$$
 (9)

should ideally exhibit plateaus for $t \ll t_{\rm max} + 2\delta t_{\rm opt} = 20a \approx 1.7 \, {\rm fm}$. We wish to check whether this is the case within the given statistics and for the quark smearing that we employ.

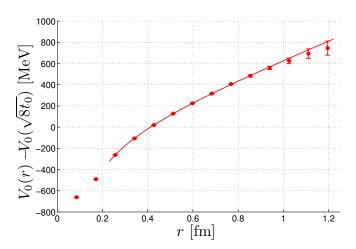


FIG. 3. The quantity $V_0(r) - V_0(\sqrt{8t_0})$, where $V_0(r)$ denotes the static quark-antiquark potential in the vacuum, together with the Cornell fit Eq. (10).

In Fig. 2 we display effective masses for some representative hadrons, namely the K^* , the nucleon N, and the cascades Ξ and Ξ^* , together with one-exponential fits to the plateau region. This region was determined from the requirement that the contribution of the second exponent of a two-exponential fit to data starting at t=3a amounted to less than 25% of the error of the correlation function. Using this criterion, indeed, in almost all the cases the plateau starts at $t<10a=2\delta t_{\rm opt}=(t_{\rm max}+2\delta t_{\rm opt})/2$. One of the few exceptions, that may very well be due to a statistical fluctuation, is the Ξ shown in the figure. We conclude that the ground state overlap achieved for the light hadrons is sufficient for our purposes.

B. The static potential in the vacuum

As described in Sec. IV, we determine the static potential, $V_0(r)$, from a variational procedure applied to a matrix of correlation functions consisting of spatially smeared Wilson loops. In Fig. 3, we show the physical quantity, $V_0(r) - V_0(\sqrt{8t_0})$, where the subtraction ensures that the self-energies of the static quarks are removed. The value of $V_0(r)$ at $r = \sqrt{8t_0}$ was obtained from a local interpolation, cf. Ref. [59]. For later use we also performed a fit to the Cornell parametrization [60]

$$V_0(r) = \mu - \frac{c}{r} + \sigma r, \qquad (10)$$

where μ denotes a constant off-set (that diverges in the continuum limit), σ is the string tension and the Coulomb coefficient reads $c=4\alpha_s/3$ at tree level. The fit with the parameter values,

$$\mu = 0.721(14) \,\text{GeV} \,, \quad c = 0.468(14) \,,$$

$$\sigma = 0.906(16) \,\text{GeV/fm} \,, \tag{11}$$

where we used $a = 0.0854 \,\mathrm{fm}$, is also shown in the figure.

To ensure that our results are not tainted by the breaking of the "string" between the static quarks, we only consider the static potential up to $\sim 1.2\,\mathrm{fm}\approx 14a$, the distance for which string breaking is expected to occur [39, 61]. At larger distances, the phenomenological parametrization Eq. (10) is no longer valid and additional interpolating operators would be required to extract the true ground state. From the static potential, we compute the static force F=V'(r) and determine the Sommer scale [62], $r_0\approx 0.5\,\mathrm{fm}$, from the equation $r^2F(r)|_{r=r_0}=1.65$, obtaining $r_0/a=5.890(41)$. We determine r_0 from a local interpolation of the static force as it is explained in [51]. Indeed, at our lattice spacing and quark mass values, $r_0\approx 5.89a\approx 5.89\times 0.0854\,\mathrm{fm}\approx 0.50\,\mathrm{fm}$.

C. The static potential within a hadron

We now determine how the presence of a hadron alters the static potential. As discussed in Sec. III, we compute correlation functions

$$C_H(r, \delta t, t) = \frac{\langle W(r, t) C_{H, 2pt}(t + 2\delta t) \rangle}{\langle W(r, t) \rangle \langle C_{H, 2pt}(t + 2\delta t) \rangle}, \qquad (12)$$

where we average over the spatial Wilson loop and hadronic sink positions, for different hadrons H. For sufficiently large values of t and for fixed values of r and δt , we can extract the difference between the static potential in the presence of the hadron, $V_H(r, \delta t) \xrightarrow{\delta t \to \infty} V_H(r)$, and the vacuum static potential, $V_0(r)$, from the exponential decay of this function in Euclidean time:

$$\Delta V_H(r, \delta t) \equiv V_H(r, \delta t) - V_0(r)$$

$$= -\lim_{t \to \infty} \frac{\mathrm{d}}{\mathrm{d}t} \ln[C_H(r, \delta t, t)]. \tag{13}$$

As the clover term that appears within the Fermionic action extends one unit in time and we have also applied one level of four-dimensional HYP smearing to the Wilson loop, we only consider $\delta t \geq 2a$. In practice, we obtain statistically meaningful results for $\delta t \leq 8a$, and in some channels even larger values are possible. Note that within Eq. (12) no variational optimization is performed but we restrict ourselves to our highest level of twelve spatial HYP smearing iterations for the Wilson loops.

For a given hadron and for each combination of r and δt , we perform linear fits in t to $\ln[C(t,\delta t,t)]$ within the effective energy plateau range. For examples see Figs. 4 and 5, where we display effective energies for the cascade and the nucleon, respectively, for $r=6a\approx 0.51\,\mathrm{fm}$ and $\delta t=5a$, together with the results of the corresponding fits. The errors are determined following Ref. [57]. Below we will assign an additional systematic error to our results from varying the fit range.

We will approximate $\Delta V_H(r)$ by $\Delta V_H(r, \delta t = 5a)$. The functional form is well described by the Cornell

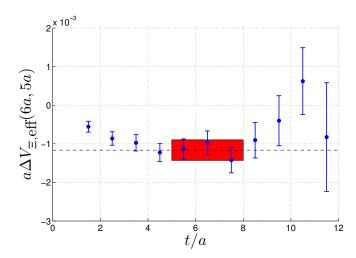


FIG. 4. Effective energy for $\Delta V_{\Xi}(r=6a, \delta t=5a)$, defined in Eqs. (12) and (13), as a function of t. For the definition of effective energies, see Eq. (9). The error band shows our estimate for $\Delta V(r, \delta t)$, obtained from a linear fit to $\ln C_H(r, \delta t, t)$.

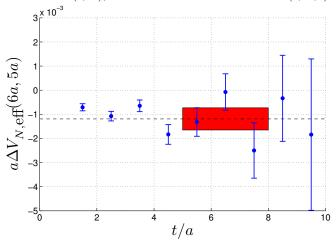


FIG. 5. The same as in Fig. 4 for the nucleon.

parametrization

$$\Delta V_H(r) = \Delta \mu_H - \frac{\Delta c_H}{r} + \Delta \sigma_H r.$$
 (14)

The errors on the fit parameters $\Delta \mu_H$, Δc_H and $\Delta \sigma_H$ which we will quote below will be indicative, since they only take into account the statistical errors of ΔV_H and neglect their correlations. Below we summarize our results for the hadron H being a pseudoscalar or vector meson, a positive parity octet or decuplet baryon and a negative parity baryon, respectively.

Note that the ρ and K^* mesons as well as the negative parity baryons are not stable for our light quark mass value and lattice volume. However, using only quarkantiquark and three-quark interpolators, we are unable to detect their decays into pairs of p-wave pions, pion plus kaon and s-wave pion plus positive parity baryon, respectively. As we see effective energy plateaus, we also quote results for these channels. Clearly, this needs to

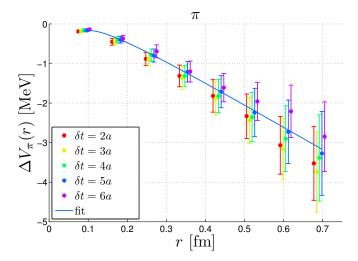


FIG. 6. The modification to the static potential in the presence of a pion, $\Delta V_{\pi}(r, \delta t)$. The colour coding corresponds to different values of δt as indicated in the legend, where the leftmost point within a group corresponds to $\delta t = 2a$. The curve shown is the result of a fit of the $\delta t = 5a$ data to Eq. (14).

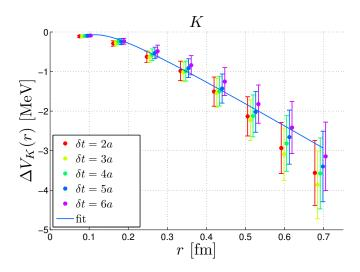


FIG. 7. The same as in Fig. 6 for the kaon.

be digested with some caution. We also note that the disconnected quark line contribution was neglected for the ϕ meson.

1. Mesons

Several hidden charm resonances such as the Y(4260) have been interpreted as tightly bound quarkonium states, embedded within light mesonic matter [21, 22]. Here we follow the procedure described above to calculate the modification of the static potential, $\Delta V_H(r, \delta t)$, for several light mesons.

In Figs. 6, 7, 8 and 9, we show our determinations for the π , the K, the K^* and the ϕ mesons, respectively, where the colour coding corresponds to different values

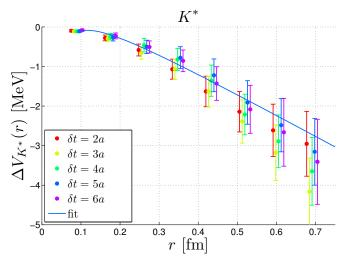


FIG. 8. The same as in Fig. 6 for the K^* meson.

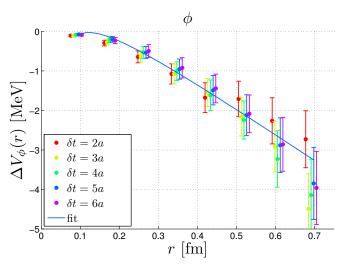


FIG. 9. The same as in Fig. 6 for the ϕ meson.

of δt which are displaced horizontally in the plots for clarity.

In all the cases we find $\Delta V_H(r,\delta t)<0$. When considering the dependence on the spatial distance between the static sources, we observe a similar pattern for all the mesons; the modification of the static potential becomes more pronounced toward large distances r. For distances up to about 0.3 fm, we generally find $|\Delta V_H(r,\delta t)|\lesssim 1\,\text{MeV}$, and at our largest shown distance of about 0.7 fm, we always find $|\Delta V_H(r,\delta t)|\lesssim 4\,\text{MeV}$. The values of $\Delta V_H(r)$ should be determined from the extrapolation $\delta t\to\infty$. In practice we find that all results for $\delta t\gtrsim 3a$ agree. The numbers obtained for $\delta t=5a$ represent a compromise between a value of δt as large as possible and a reasonable signal-to-noise ratio. These should be considered as our final results and are displayed in Table I.

Our data are well described by the parametrization given in Eq. (14). The resulting fit parameters for the

| TABLE I. | Values of the | difference i | n the | static | potential | for t | the m | nesons, | measured | at $\delta t =$ | 5a. | Errors a | re stati | stical | and |
|-------------|---------------|--------------|-------|-------------------------|-----------|-------|-------|---------|----------|-----------------|-----|----------|----------|--------|-----|
| systematic, | respectively. | | | | | | | | | | | | | | |

| r/a | $\Delta V_{\pi} [\mathrm{MeV}]$ | $\Delta V_K [{ m MeV}]$ | $\Delta V_{ ho} [{ m MeV}]$ | $\Delta V_{K^*} [\mathrm{MeV}]$ | $\Delta V_{\phi} [\mathrm{MeV}]$ |
|-----|-----------------------------------|---------------------------|-------------------------------|---------------------------------|------------------------------------|
| 1 | -0.16(3)(1) | -0.10(3)(1) | -0.07(6)(5) | -0.11(3)(3) | -0.08(2)(3) |
| 2 | -0.40(8)(4) | -0.24(8)(3) | -0.17(17)(20) | -0.27(8)(7) | -0.22(7)(6) |
| 3 | -0.80(16)(19) | -0.53(14)(09) | -0.29(33)(56) | -0.50(17)(08) | -0.49(16)(9) |
| 4 | -1.21(26)(30) | -0.91(24)(18) | -0.46(52)(1.03) | -0.78(28)(21) | -0.85(26)(22) |
| 5 | -1.71(40)(56) | -1.43(37)(27) | -0.67(73)(1.24) | -1.22(41)(45) | -1.39(38)(49) |
| 6 | -2.24(61)(71) | -2.02(51)(45) | -1.33(96)(2.09) | -1.91(55)(83) | -2.09(52)(80) |
| 7 | -2.73(80)(86) | -2.66(68)(71) | -2.03(1.20)(3.19) | -2.48(67)(1.36) | -2.78(66)(1.38) |
| 8 | -3.27(1.06)(63) | -3.40(89)(1.02) | -2.77(1.46)(4.75) | -3.15(84)(2.24) | -3.43(84)(2.10) |

TABLE II. Fit parameters for the difference of the potential for the mesons, see Eq. (14).

| Meson H | $\Delta\mu_H [\mathrm{MeV}]$ | $\Delta c_H \left[10^{-4} \right]$ | $\Delta \sigma_H [\mathrm{MeV}/ \mathrm{fm}]$ |
|-------------|------------------------------|-------------------------------------|---|
| π | 0.858(39) | 2.30(13) | -5.75(11) |
| K | 1.167(15) | 3.34(52) | -5.82(42) |
| ho | 2.28(38) | 6.62(1.31) | -10.19(1.02) |
| K^{\star} | 1.38(16) | 4.10(59) | -6.47(46) |
| ϕ | 1.45(12) | 4.18(42) | -6.67(32) |

different mesons are displayed in Table II and the corresponding curves are also shown in the figures. Note that, although the fit parameters appear to indicate a somewhat different behaviour for the ρ meson, the data points alone, that are displayed in Table I, do not show any statistically significant deviation.

We will take the analysis one step further in Sec. VI. However, taking the above results at face value, we can already make two interesting observations. The first one is that, for identical valence quark content, there is no difference between the tendency of light pseudoscalars, such as the pion or the kaon, and vector mesons, such as the ρ or the K^* , to bind with quarkonium. The second observation is that there appears to be little or no difference increasing or decreasing the strangeness of the light mesonic matter.

2. Positive parity baryons

We now turn our attention to modifications of the static potential in the presence of a positive parity octet $(J^P=1/2^+)$ or decuplet $(J^P=3/2^+)$ baryon. As explained at the end of Sec. IV, in the latter case we are restricted to employing a particular polarization to avoid mixing with J=1/2 states. In our case we project onto $J_z=3/2$ with respect to the z axis. We remark that embedding charmonium states within baryons of vanishing strangeness could be an interpretation of the "pentaquark" structures that were recently reported by the LHCb Collaboration [1,2], for examples see the last paragraph of Sec. III.

In Figs. 10, 11, 12 and 13 we show $\Delta V_H(r, \delta t)$ for the

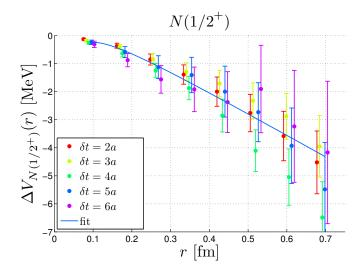


FIG. 10. The same as in Fig. 6 for the positive parity nucleon.

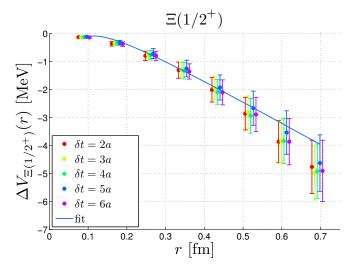


FIG. 11. The same as in Fig. 6 for the positive parity cascade.

nucleon, the cascade Ξ , the Δ and the decuplet cascade Ξ^* , respectively. Again, in all the cases we observe $\Delta V_H(r, \delta t) < 0$. The results for the positive parity baryons are collected in Table III and are very similar to the values discussed above for the pseudoscalar and

-5.70(1.23)(2.24)

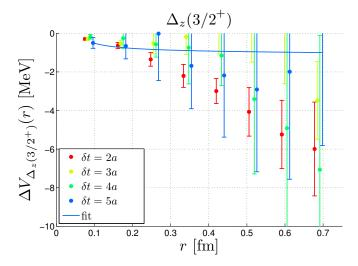
-7.35(1.66)(3.37)

| r/a | $\Delta V_{N(1/2^+)} [\mathrm{MeV}]$ | $\Delta V_{\Sigma(1/2^+)} [\mathrm{MeV}]$ | $\Delta V_{\Lambda(1/2^+)} [\mathrm{MeV}]$ | $\Delta V_{\Xi(1/2^+)} [\mathrm{MeV}]$ |
|-----|---|---|--|---|
| 1 | -0.24(8)(13) | -0.12(3)(10) | -0.24(4)(5) | -0.12(3)(5) |
| 2 | -0.58(19)(33) | -0.32(9)(20) | -0.60(10)(15) | -0.33(8)(9) |
| 3 | -1.12(41)(68) | -0.67(20)(38) | -1.12(22)(29) | -0.72(18)(15) |
| 4 | -1.40(63)(72) | -1.22(32)(33) | -1.64(35)(28) | -1.25(30)(22) |
| 5 | -1.99(91)(67) | -2.03(49)(54) | -2.49(60)(46) | -1.93(44)(40) |
| 6 | -2.73(1.05)(1.08) | -2.87(68)(91) | -3.21(80)(59) | -2.67(61)(51) |
| 7 | -3.93(1.35)(1.53) | -3.62(90)(1.08) | -4.19(1.00)(1.30) | -3.54(78)(1.00) |
| 8 | -5.48(1.67)(2.28) | -4.40(1.16)(1.47) | -5.34(1.23)(1.84) | -4.63(1.01)(1.80) |
| | $\Delta V_{\Delta(3/2^+)} [\mathrm{MeV}]$ | $\Delta V_{\Sigma^{\star}(3/2^{+})} [\mathrm{MeV}]$ | $\Delta V_{\Xi^{\star}(3/2^{+})} [\mathrm{MeV}]$ | $\Delta V_{\Omega(3/2^+)} [\mathrm{MeV}]$ |
| 1 | -0.50(28)(46) | -0.23(9)(7) | -0.18(6)(5) | -0.15(4)(5) |
| 2 | -0.65(66)(58) | -0.49(24)(13) | -0.47(14)(20) | -0.40(10)(16) |
| 3 | -0.01(2.43)(1.29) | -1.27(52)(31) | -1.04(29)(48) | -0.91(22)(40) |
| 4 | -1.68(2.22)(1.22) | -1.96(84)(45) | -1.53(46)(72) | -1.45(37)(70) |
| 5 | -2.18(3.20)(3.04) | -3.27(1.18)(65) | -2.12(67)(99) | -2.07(53)(1.22) |
| 6 | -2.91(4.26)(3.64) | -5.33(2.81)(1.65) | -3.47(1.50)(1.04) | -3.31(1.00)(1.41) |

-5.41(2.09)(1.86)

-6.14(2.79)(2.02)

TABLE III. Values of the difference in the static potential for the positive parity baryons, measured at $\delta t = 5a$.



-1.99(5.75)(2.12)

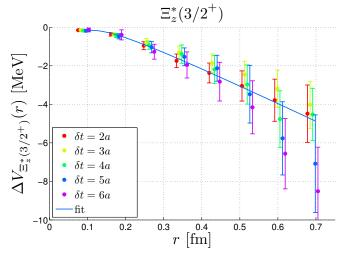
9.5(15.3)(11.4)

7

FIG. 12. The same as in Fig. 6 for the positive parity Δ baryon. The subscript z of the baryon label refers to the projection along the z axis $J_z=3/2$, ensuring no mixing with $J^P=1/2^+$ states takes place.

TABLE IV. Fit parameters for the difference of the potential for the positive parity baryons, see Eq. (14).

| Baryon H | $\Delta\mu_H [\mathrm{MeV}]$ | $\Delta c_H [10^{-4}]$ | $\Delta \sigma_H [\mathrm{MeV}/ \mathrm{fm}]$ |
|---------------------------------|------------------------------|-------------------------|---|
| $N(1/2^{+})$ | 1.17(37) | 3.21(1.30) | -7.83(97) |
| $\Sigma (1/2^+)$ | 1.62(21) | 4.63(73) | -7.99(60) |
| $\Lambda \left(1/2^{+}\right)$ | 1.28(20) | 3.46(69) | -8.49(57) |
| $\Xi(1/2^{+})$ | 1.54(19) | 4.32(75) | -7.81(55) |
| $\Delta \left(3/2^{+} \right)$ | -0.99(1.75) | -2.22(6.16) | -0.10(4.77) |
| $\Sigma^{\star} (3/2^{+})$ | 2.15(37) | 6.14(1.30) | -11.38(1.01) |
| $\Xi^{\star} (3/2^{+})$ | 1.74(36) | 4.90(1.41) | -9.40(1.03) |
| $\Omega\left(3/2^+\right)$ | 2.34(49) | 6.77(1.68) | -11.02(1.41) |



-5.76(1.90)(1.87)

-7.08(2.53)(3.02)

FIG. 13. The same as in Fig. 12 for the positive parity Ξ^* baryon.

vector mesons. Note however, that the errors of ΔV in the presence of decuplet baryons become rather large. In particular, this is so for the Δ , which is why in this case we only show the data up to $\delta t = 5a$. The Cornell fit parameters Eq. (14) are displayed in Table IV.

3. Negative parity baryons

The modification of the potential in the presence of negative parity baryons appears statistically consistent to the positive parity case, however, due to the much larger statistical errors, we cannot exclude a more rapid decrease of $\Delta V_H(r)$ as a function of r. As examples we show in Figs. 14, 15 and 16 the results for the negative parity partners of the nucleon, the cascade and the decu-

| | | * | to negative parity saryons, mea | |
|-----|---|---|--|---|
| r/a | $\Delta V_{N(1/2^-)} [\mathrm{MeV}]$ | $\Delta V_{\Sigma(1/2^-)} [\mathrm{MeV}]$ | $\Delta V_{\Lambda(1/2^-)} [\mathrm{MeV}]$ | $\Delta V_{\Xi(1/2^-)} [\mathrm{MeV}]$ |
| 1 | -1.73(91)(43) | -0.68(50)(77) | -1.09(48)(95) | -0.31(26)(29) |
| 2 | -4.19(2.30)(1.74) | -1.46(1.27)(1.61) | -2.59(1.24)(1.92) | -0.60(69)(51) |
| 3 | -8.43(5.48)(4.19) | -2.93(2.59)(3.16) | -5.31(2.69)(3.68) | -1.13(1.41)(58) |
| 4 | -12.27(7.53)(5.25) | -5.12(4.06)(4.76) | -8.08(4.12)(6.48) | -3.29(2.28)(2.08) |
| 5 | -12.7(11.4)(9.7) | -6.21(6.01)(6.09) | -12.1(6.1)(10.1) | -5.28(3.32)(3.80) |
| 6 | 1.1(12.7)(22.9) | -5.80(8.06)(5.20) | -14.2(6.4)(9.6) | -8.93(4.61)(6.57) |
| 7 | 4.6(18.7)(31.8) | -7.3(10.2)(5.9) | -7.36(6.80)(7.91) | -9.16(5.75)(6.29) |
| 8 | 0.9(24.8)(35.4) | -9.1(12.9)(7.1) | -3.9(8.8)(19.5) | -6.65(7.10)(5.83) |
| | $\Delta V_{\Delta(3/2^-)} [\mathrm{MeV}]$ | $\Delta V_{\Sigma^{\star}(3/2^{-})} [\mathrm{MeV}]$ | $\Delta V_{\Xi^{\star}(3/2^{-})} [\mathrm{MeV}]$ | $\Delta V_{\Omega(3/2^-)} [\mathrm{MeV}]$ |
| 1 | 0.98(7.20)(1.66) | -0.70(1.22)(0.28) | 0.01(28)(25) | -0.11(20)(10) |
| 2 | 0.1(16.7)(7.5) | -3.74(4.87)(1.49) | -1.72(1.52)(1.02) | -0.46(47)(13) |
| 3 | 1.0(29.2)(16.1) | -8.06(5.46)(3.29) | -2.47(2.17)(1.57) | -0.64(96)(55) |
| 4 | 49.3(64.4)(7.6) | -13.8(8.5)(3.9) | -2.47(1.79)(0.83) | -0.48(1.50)(1.30) |
| 5 | 35.8(95.8)(12.5) | -12.6(6.8)(12.6) | -3.26(2.48)(3.05) | 0.01(2.11)(2.11) |
| 6 | 56.9(96.8)(17.2) | -11.0(32.4)(4.3) | -4.35(3.19)(5.40) | -0.46(2.87)(2.76) |
| 7 | 1.4(132.0)(34.6) | -8.1(42.7)(9.7) | -6.06(3.99)(5.70) | -1.62(3.73)(2.77) |
| 8 | -25.6(160.0)(49.7) | -21.5(13.2)(11.9) | -8.09(4.90)(6.33) | -3.33(4.77)(3.23) |

TABLE V. Values of the difference in the static potential for the negative parity baryons, measured at $\delta t = 5a$.

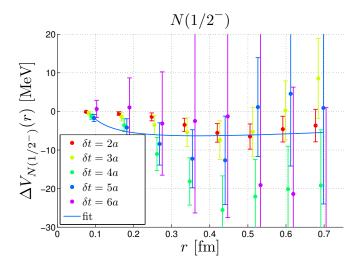


FIG. 14. The same as in Fig. 6 for the negative parity nucleon.

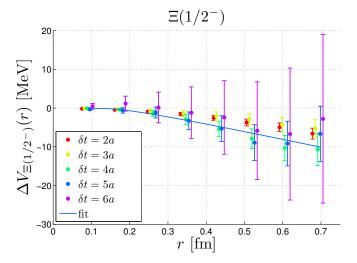


FIG. 15. The same as in Fig. 6 for the negative parity cascade.

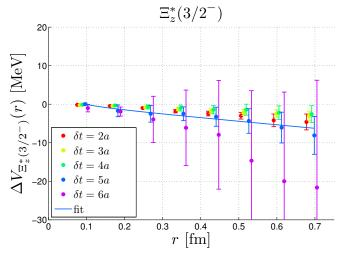


FIG. 16. The same as in Fig. 12 for the negative parity Ξ^* baryon.

plet cascade, respectively. The corresponding numerical values for $\delta t=5a$ are displayed in Table V and the Cornell fit parameters in Table VI.

4. Summary

Regardless of meson or baryon, spin, strangeness or parity, the modifications of the static potential are well described by the parametrization Eq. (14), with the main effects being a reduction of the linear slope and increases of the Coulomb coefficient c and of the off-set μ . All data are consistent with a decrease of the static potential at the distance $r=0.5\,\mathrm{fm}$ by about 2–3 MeV.

For r > 0.7 fm the statistical errors grow substantially as a result of the deteriorating signal-to-noise ratio. For-

TABLE VI. Fit parameters for the difference of the potential for the negative parity baryons, see Eq. (14).

| Baryon H | $\Delta\mu_H [\mathrm{MeV}]$ | $\Delta c_H \left[10^{-4} \right]$ | $\Delta \sigma_H [\mathrm{MeV/fm}]$ |
|----------------------------------|--------------------------------|-------------------------------------|---------------------------------------|
| $N(1/2^{-})$ | -10.18(6.43) | -3.50(22.58) | 5.39(17.46) |
| $\Sigma \left(1/2^{-1}\right)$ | 1.88(83) | 4.84(2.91) | -16.89(2.26) |
| $\Lambda \left(1/2^{-} \right)$ | -0.77(3.51) | -5.03(12.61) | -16.92(8.93) |
| $\Xi(1/2^{-1})$ | 4.74(1.18) | 14.21(4.11) | -20.93(3.25) |
| $\Delta (3/2^{-})$ | -23.1(27.6) | -69.34(96.85) | 94.8(76.2) |
| $\Sigma^{\star} (3/2^{-})$ | -0.853(3.26) | -12.11(11.90) | -30.3(7.22) |
| $\Xi^{\star} (3/2^{-})$ | -0.23(1.25) | -4.37(4.59) | -8.92(2.61) |
| $\Omega \left(3/2^{-} \right)$ | -0.47(62) | -1.92(2.18) | -0.99(1.67) |

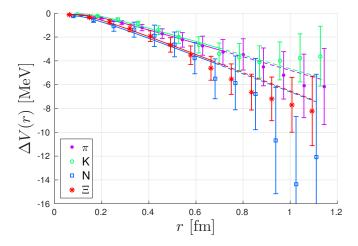


FIG. 17. The difference in the static potential for the pion, the kaon and the positive parity nucleon and cascade, measured at $\delta t = 5a$, up to a distance of 1.2 fm. The curves correspond to the parametrization Eq. (14) with the parameters (obtained by fitting the r < 0.7 fm data points) displayed in Tables II and IV.

tunately, larger distances exceed the size both of charmonium and of the hosting hadron and will not be relevant for the discussion of Sec. VI below. However, one may wonder if the reduction persists. In Fig. 17 we show the data for the pion, the kaon, the nucleon and the cascade up to $r\approx 1.2$ fm, a distance around which string breaking will occur [39, 61]. The decrease of the slope appears to be robust and all large distance data points are consistent with our parametrizations. However, for the more compact pseudoscalar mesons and in particular the kaon the data suggests that above $r\approx 0.8$ fm some saturation may set in.

VI. MODIFICATION OF CHARMONIUM BINDING ENERGIES

We have investigated how the static quark-antiquark potential changes in the presence of a light hadron. This is a well-defined observable and the results by themselves are already interesting. However, we wish to go one step further and address possible phenomenological consequences. We start with a few words of caution. When it comes to charmonia (and even for bottomonia), relativistic corrections are not small. Moreover, baryons are not particularly light in comparison to the charm quark. Therefore, for charmonia it may be doubtful if their effect can be completely integrated out in a Born-Oppenheimer or adiabatic spirit and put into the quark-antiquark interaction potential. This is less of a problem for the pion and the kaon since M_K/m_c and M_π/m_c are of similar sizes as the squared velocity $v^2 \sim 0.3$. In what follows, we will neglect these effects.

We start from the Schrödinger equation

$$\left[-\frac{\nabla^2}{m_c} + E_H(r) \right] \psi_{nL}^{(H)}(r, \theta, \phi) = M_{nL}^{(H)} \psi_{nL}^{(H)}(r, \theta, \phi) ,$$
(15)

where the reduced mass is $m_c/2$ and

$$E_H(r) = 2(m_c - \delta m) + V_H(r) \tag{16}$$

$$= 2m_c + v_0 + \Delta \mu_H - \frac{c_H}{r} + \sigma_H r.$$
 (17)

In the second step, we have assumed the Cornell parametrization given by Eqs. (10) and (14), where we set $c_H = c + \Delta c_H$ and $\sigma_H = \sigma + \Delta \sigma_H$. The parameters $\Delta \mu_H$, Δc_H and $\Delta \sigma_H$ specify the modifications of the constant, the Coulomb and the linear terms, respectively, obtained from the Cornell fits to $\Delta V_H(r) = V_H(r) - V_0(r)$ carried out in the previous section.

The Cornell parametrization is not valid at large distances due to string breaking effects [39, 61] or at small distances where one would expect the coefficient c_H to run with the scale r. However, we are only interested in mass differences $\Delta M_{nL}^{(H)} = M_{nL}^{(H)} - M_{nL}^{(0)}$ between a charmonium state with radial and angular momentum quantum numbers n and L respectively, in the presence of a hadron H, relative to the same state in the vacuum. We expect such corrections to affect both masses in similar ways, and therefore to cancel from these differences. The coefficients $\Delta \mu_H$, c_H and σ_H are taken from the fits performed in the previous section, while the mass parameter m_c and the offset $v_0 = \mu - 2\delta m$ have to be fixed by matching the energy levels $M_{nL} = M_{nL}^{(0)}$, obtained from solving the above Schrödinger equation, to experiment.

Due to the approximations made, our discussion can only be qualitative and hence we neglect our statistical and systematic uncertainties. The central values for the parameters from the Cornell fit to the static potential in the vacuum read (see also Eq. (11)),

$$\sigma = 0.0335a^{-2} \approx (423 \,\text{MeV})^2 , \quad c = 0.468 \,.$$
 (18)

Numerically solving the Schrödinger equation and adjusting m_c and v_0 so that we reproduce the spin averaged 1S and 2S charmonium levels, we find

$$m_c = 1269 \,\text{MeV} \,, \quad v_0 = 113 \,\text{MeV} \,.$$
 (19)

From Table VII, we see that the above parameters indeed reproduce the experimental 1S and 2S levels, however, we underestimate the 1P mass by $42\,\text{MeV}$. This is due to a combination of overestimating the value of the wave function at the origin, as we neglected running coupling effects, and relativistic corrections [63]; within our approximations, it is not possible to simultaneously reproduce all spin-independent mass splittings within an accuracy better than about 10%.

A negative value of $\Delta M_{nL}^{(H)}$ means that embedding a charmonium state within the hadron H is energetically favourable, which we interpret as attraction. Unlike in the hydrogen case, the potential is only bound from above by the $D\overline{D}$ threshold and so it may not be entirely obvious whether a negative $\Delta V_H(r)$ results in a positive or a negative shift of the charmonium mass. On one hand, a lower V_H results in a lower E_H and therefore in a smaller $M_{nL}^{(H)}$ mass. On the other hand, the slope is reduced, resulting in a more extended and less strongly bound wave function.

Before numerically solving the Schrödinger equation we investigate a toy model with a purely linear potential $V(r) = \sigma r$. The virial theorem then gives a kinetic energy

$$2\langle T \rangle = \langle r \, dV / dr \rangle = \sigma \langle r \rangle = 2M - 2\sigma \langle r \rangle, \qquad (20)$$

where we used $M=\langle T\rangle+\langle V\rangle=\langle T\rangle+\sigma\langle r\rangle$. This means that $\langle r\rangle=2M/(3\sigma)$. The Feynman–Hellmann theorem then gives

$$\frac{\partial M}{\partial \sigma} = \left\langle \frac{\partial H}{\partial \sigma} \right\rangle = \left\langle r \right\rangle = \frac{2M}{3\sigma} \,, \tag{21}$$

i.e.

$$\Delta M^{(H)} = (\sigma_H - \sigma) \left. \frac{\partial M}{\partial \sigma} \right|_{\sigma = \sigma_0} = \frac{2\sigma_H}{3\sigma_0} M^{(0)}, \quad (22)$$

where $M^{(H)}=M(\sigma_H)$. Therefore, we expect the part of the mass which is due to the interaction, $M-2(m_c-\delta m)$, to be lowered by a factor $2\sigma_H/(3\sigma)$, which for our data typically amounts to about 0.4%. As we have neglected Coulomb interactions, we should also neglect the self-energy δm . Then, using the m_c value of Eq. (19) and $M_{1S}=3069\,\mathrm{MeV}$, this difference gives 530 MeV. So, for the 1S state, we expect an attraction $\Delta M_{1S}^{(H)}\approx -2\,\mathrm{MeV}$. Using the experimental 1P–1S and 2S–1S differences lowers this to $\Delta M_{1P}^{(H)}\approx -3.9\,\mathrm{MeV}$ and $\Delta M_{2S}^{(H)}\approx -4.5\,\mathrm{MeV}$, respectively.

We now solve the Schrödinger equation numerically for the mesons and for some of the positive parity baryons, using the parameter values of Eqs. (18) and (19), together with $\Delta \mu_H$, Δc_H and $\Delta \sigma_H$ obtained from the fits to $\Delta V_H(r)$, see Tables II and IV. The results are collected in Table VII. Indeed, the masses in all the channels shown are lowered by amounts that are in qualitative agreement with the considerations from the virial and Feynman–Hellmann theorems above, and the effect becomes larger for spatially more extended charmonia. Note that the potentials for the ρ meson and the Δ baryon have relatively large errors. Therefore, the resulting mass shifts

TABLE VII. Masses and mass differences of spin-averaged states in MeV taken from experiment [43] and from solving the Schrödinger equation using the Cornell parametrization of our lattice results.

| Mass/Mass difference | $1S [\mathrm{MeV}]$ | $1P[\mathrm{MeV}]$ | $2S [\mathrm{MeV}]$ |
|------------------------|-----------------------|--------------------|-----------------------|
| M_{nL} (experiment) | 3068.6 | 3525.3 | 3674.4 |
| M_{nL} (Schrödinger) | 3068.6 | 3483.3 | 3674.4 |
| $\Delta M^{(\pi)}$ | -1.7 | -3.1 | -4.0 |
| $\Delta M^{(K)}$ | -1.5 | -2.9 | -3.8 |
| $\Delta M^{(ho)}$ | -2.5 | -4.9 | -6.5 |
| $\Delta M^{(K^*)}$ | -1.6 | -3.2 | -4.2 |
| $\Delta M^{(\phi)}$ | -1.6 | -3.2 | -4.3 |
| $\Delta M^{(N)}$ | -2.4 | -4.3 | -5.5 |
| $\Delta M^{(\Xi)}$ | -2.0 | -3.9 | -5.1 |
| $\Delta M^{(\Delta)}$ | -0.9 | -1.0 | -1.0 |
| $\Delta M^{(\Xi^*)}$ | -2.6 | -4.8 | -6.3 |

statistically agree with those shown for the K^* and the Ξ^* , respectively.

In Ref. [35], a charmonium-nucleon bound state energy of $-20\,\mathrm{MeV}$ was reported — a factor of eight larger than our result. The light quark mass employed in that study was approximately 13 times larger than the one we use here. However, as one can see from Table VII, if we replace the nucleon by the cascade that contains two strange quarks, which are eight times heavier than our light quark, the binding appears to become even weaker, albeit by a statistically insignificant difference.

We found that, within the approximations made, the binding of the charmonium 1S state becomes stronger by values ranging from $-1\,\mathrm{MeV}$ to $-2.5\,\mathrm{MeV}$. For the 2S state this effect increases to $-1\,\mathrm{MeV}$ to $-6.5\,\mathrm{MeV}$. Such estimates will be more reliable for bottomonia where relativistic and m_H/m_b corrections are smaller. However, these states are also less extended spatially and $V_0(r)$ is most strongly modified towards large distances. This means that the mass shifts induced by the presence of a light hadron will be even smaller in the bottomonium case since charmonium and bottomonium binding energies $\sim m_O v^2$ are of similar sizes.

VII. SUMMARY AND OUTLOOK

Studying charmonium resonances above strong decay thresholds poses a considerable challenge to lattice QCD. In most cases not only radial excitations of the charm quark-antiquark system need to be resolved but also several decay channels open up, at least near the physical values of the light quark mass. Some of the relevant thresholds involve the scattering of three and more hadrons. In this case even the required methodology is under active development — for recent progress in this direction, see Refs. [64–69]. In view of this, testing specific models or making assumptions in certain limiting cases represents a viable alternative and may provide at

least some first principles insight into the nature of exotic bound states containing hidden charm.

Here we have investigated in the heavy quark limit the hadro-quarkonium picture [21], which assumes quarkonium can be bound inside the core of a light hadron. We employed a single CLS [44] ensemble with $N_f = 2 + 1$ flavours of non-perturbatively order-a improved Wilson quarks at a lattice spacing $a \approx 0.085 \,\mathrm{fm}$. The pion and kaon masses are approximately 223 MeV and 476 MeV, respectively, i.e. the light quark mass is by a factor of about 2.7 larger than in nature. Our approach for testing this picture was first to determine the potential between a pair of static sources, approximating a heavy quark-antiquark pair, in the absence of the hadron. Assuming the non-relativistic limit, the Schrödinger equation can then be solved with this potential in order to obtain (spin-averaged) quarkonium energy levels. This approach can be extended systematically, adding v^2 corrections, to include heavy quark spin and momentum dependent effects [70–75]. Making the additional assumption that the heavy quark mass is much larger than the mass of the light hadron, the effect of the light hadron onto the quarkonium can also be integrated out adiabatically and cast into the quark-antiquark interaction potential.

We calculated such potentials in the background of a hadron H for a variety of pseudoscalar and vector mesons, octet and decuplet baryons and their negative parity partners. Of particular interest are the differences $\Delta V_H(r)$, relative to the potential in the vacuum. Solving the Schrödinger equation with the modified potential and comparing the outcome to the results obtained in vacuo provides an indication of the strength of the binding between the host hadron and the quarkonium, at least in the heavy quark limit. In principle this approach can also be extended, including mass dependent corrections and interactions between the spins of the hadron and the heavy quarks. As the effects we detected were quite small, we have however no immediate plans of pursuing this line of research.

Resolving very small energy differences was possible by employing a large number of sources on 1552 gauge configurations, corresponding to over 6000 molecular dynamics units of the hybrid Monte Carlo algorithm. For all the light mesons, namely the π , K, ρ , K^{\star} and ϕ , as well as the baryons we considered, namely the N, Σ, Λ, Ξ , Δ, Σ^*, Ξ^* and Ω of both parities, we found $\Delta V_H(r) < 0$, suggesting a tendency to bind. The main effect could be quantified as a reduction of the linear slope of the potential. At a distance of 0.5 fm the potential was lowered by only 2–3 MeV for all these hadrons. Increasing the strangeness resulted in smaller statistical errors but differences between the investigated hadrons were not significant. Translating the modification of the potential into energy levels by solving the Schrödinger equation suggested values for the finite volume binding energy of 1S charmonium ranging from $-1\,\mathrm{MeV}$ to $-2.5\,\mathrm{MeV}$ and 2S charmonium from -1 to $-6.5\,\mathrm{MeV}$, see Table VII.

These effects should be even smaller for bottomonia that are most sensitive to modifications of the potential at very short distances.

These binding energies are similar in size to that of deuterium and may be hard to reconcile with the hadro-quarkonium picture where the quarkonium is thought to be localized inside the light hadron which has a size $\lesssim 1\,\mathrm{fm}$. Therefore, in the heavy quark limit, that should at least apply to bottomonia, this may not be a viable picture. We cannot exclude, however, different mechanisms to stabilize hadro-charmonia such as relativistic corrections or corrections due to the mass of the hosting hadron.

The spatial lattice extent $L \approx 4.6/M_{\pi} \approx 4.1 \,\mathrm{fm}$ was not only large relative to the inverse pion mass but also in comparison to the size of a light hadron or a quarkonium state; however, the observed effects were very small. Hence, a finite volume study (see, e.g., Ref. [33]) is required to establish if the reported binding energies survive the infinite volume limit. Simulations on different volumes, and also injecting momentum to enable a scattering study, are ongoing, see Ref. [76] for preliminary results. Until these more extensive investigations are concluded, we cannot exclude the possibility that no bound state or resonance exists. Therefore, the binding energies presented here should only be considered as upper limits.

ACKNOWLEDGMENTS

This work was supported by the Deutsche Forschungsgemeinschaft (DFG) Grant No. SFB/TRR 55. G.M. acknowledges support from the Herchel Smith Fund at the University of Cambridge and the DFG under Contract No. KN 947/1-2. The ensemble C101 was generated by CLS [44] employing the OPENQCD [45, 46] software and using computer time provided by PRACE (Partnership for Advanced Computing in Europe, http://www. prace-ri.eu) on Fermi at CINECA Bologna and on SuperMUC at Leibniz Supercomputing Centre Munich. An additional stream was generated on the "Clover" Cluster of the Mainz Helmholtz Institute. Analysis was performed on the SFB/TRR 55 QPACE 2 [77] Xeon-Phi installation at Regensburg and on the Stromboli cluster in Wuppertal. We used the CHROMA [78] software package along with the LIBHADRONANALYSIS library and the multigrid solver implementation of Ref. [79] (see also Refs. [80–82]) to generate hadronic two-point functions. Wilson loops were generated using Björn Leder's WLOOP package [50, 51]. For the error analysis we used the software of the ALPHA collaboration [57, 58] available at http://www-zeuthen.desy.de/alpha/. We thank Peter Georg, Benjamin Gläßle and Daniel Richtmann for support. Last but not least we thank all our CLS colleagues and in particular Dalibor Djukanovic, Georg Engel and Leonardo Giusti for generating the C101 ensemble and Stefan Schaefer for coordinating the CLS simulations.

- [1] Roel Aaij et al. (LHCb Collaboration), "Observation of $J/\psi\rho$ resonances consistent with pentaquark states in $\Lambda_b^0 \to J/\psi K^- p$ decays," Phys. Rev. Lett. **115**, 072001 (2015), arXiv:1507.03414 [hep-ex].
- [2] Roel Aaij et al. (LHCb Collaboration), "Model-independent evidence for $J/\psi p$ contributions to $\Lambda_b^0 \to J/\psi p K^-$ decays," Phys. Rev. Lett. **117**, 082002 (2016), arXiv:1604.05708 [hep-ex].
- [3] Adam P. Szczepaniak, "Dalitz plot distributions in presence of triangle singularities," Phys. Lett. B 757, 61 (2016), arXiv:1510.01789 [hep-ph].
- [4] Feng-Kun Guo, Ulf-G. Meißner, Juan Nieves, and Zhi Yang, "Remarks on the P_c structures and triangle singularities," Eur. Phys. J. A 52, 318 (2016), arXiv:1605.05113 [hep-ph].
- [5] Nora Brambilla et al. (Quarkonium Working Group), "Heavy quarkonium: progress, puzzles, and opportunities," Eur. Phys. J. C 71, 1534 (2011), arXiv:1010.5827 [hep-ph].
- [6] Hua-Xing Chen, Wei Chen, Xiang Liu, and Shi-Lin Zhu, "The hidden-charm pentaquark and tetraquark states," Phys. Rept. 639, 1 (2016), arXiv:1601.02092 [hep-ph].
- [7] Robert L. Jaffe, "Multi-quark hadrons. 1. The phenomenology of qqqq mesons," Phys. Rev. D 15, 267 (1977).
- [8] John D. Weinstein and Nathan Isgur, "Do multi-quark hadrons exist?" Phys. Rev. Lett. 48, 659 (1982).
- [9] Luciano Maiani, Antonio D. Polosa, and Veronica Riquer, "Indications of a four-quark structure for the X(3872) and X(3876) particles from recent Belle and BABAR data," Phys. Rev. Lett. **99**, 182003 (2007), arXiv:0707.3354 [hep-ph].
- [10] Stanley J. Brodsky, Dae Sung Hwang, and Richard F. Lebed, "Dynamical picture for the formation and decay of the exotic XYZ mesons," Phys. Rev. Lett. 113, 112001 (2014), arXiv:1406.7281 [hep-ph].
- [11] Richard F. Lebed, "How Often Do Diquarks Form? A Very Simple Model," Phys. Rev. D 94, 034039 (2016), arXiv:1606.07108 [hep-ph].
- [12] Mikhail B. Voloshin and Lev B. Okun, "Hydronic molecules and the charmonium atom," JETP Lett. 23, 333 (1976), [Pisma Zh. Eksp. Teor. Fiz. 23, 369 (1976)].
- [13] Alvaro De Rújula, Howard Georgi, and Sheldon L. Glashow, "Molecular charmonium: A new spectroscopy?" Phys. Rev. Lett. 38, 317 (1977).
- [14] Victor A. Novikov, Lev B. Okun, Mikhail A. Shif-man, Arkady I. Vainshtein, Mikhail B. Voloshin, and Valentin I. Zakharov, "Charmonium and gluons: Basic experimental facts and theoretical introduction," Phys. Rept. 41, 1 (1978).
- [15] Nils A. Törnqvist, "From the deuteron to deusons, an analysis of deuteron-like meson meson bound states," Z. Phys. C. 61, 525 (1994), arXiv:hep-ph/9310247 [hep-ph].
- [16] Frank Close, Clark Downum, and Christopher E. Thomas, "Novel charmonium and bottomonium spectroscopies due to deeply bound hadronic molecules from single pion exchange," Phys. Rev. D 81, 074033 (2010), arXiv:1001.2553 [hep-ph].
- [17] Ted Barnes, "Colored quark and gluon constituents in the MIT bag model," Nucl. Phys. B 158, 171 (1979).

- [18] Ted Barnes and Frank E. Close, "A light exotic $q\bar{q}g$ hermaphrodite meson?" Phys. Lett. **116B**, 365 (1982).
- [19] Michael S. Chanowitz and Stephen R. Sharpe, "Hybrids: Mixed states of quarks and gluons," Nucl. Phys. B 222, 211 (1983), [Erratum: Nucl. Phys. B 228, 588 (1983)].
- [20] Nathan Isgur, Richard Kokoski, and Jack Paton, "Gluonic excitations of mesons: Why they are missing and where to find them," Proceedings, International Conference on Hadron Spectroscopy, Phys. Rev. Lett. 54, 869 (1985), [AIP Conf. Proc. 132, 242 (1985)].
- [21] S. Dubynskiy and Mikhail B. Voloshin, "Hadro-charmonium," Phys. Lett. B 666, 344 (2008), arXiv:0803.2224 [hep-ph].
- [22] Xin Li and Mikhail B. Voloshin, "Y(4260) and Y(4360) as mixed hadrocharmonium," Mod. Phys. Lett. A **29**, 1450060 (2014), arXiv:1309.1681 [hep-ph].
- [23] Martin Lüscher, "Two particle states on a torus and their relation to the scattering matrix," Nucl. Phys. B 354, 531 (1991).
- [24] Sasa Prelovsek, "Lattice studies of charmonia and exotics," in 7th International Workshop on Charm Physics (Charm 2015) Detroit, MI, USA, May 18-22, 2015 (2015) arXiv:1508.07322 [hep-lat].
- [25] William E. Caswell and G. Peter Lepage, "Effective Lagrangians for bound state problems in QED, QCD, and other field theories," Phys. Lett. B 167, 437 (1986).
- [26] Antonio Pineda and Joan Soto, "Effective field theory for ultrasoft momenta in NRQCD and NRQED," Quantum chromodynamics. Proceedings, Conference, QCD'97, Montpellier, France, July 3-9, 1997, Nucl. Phys. Proc. Suppl. 64, 428 (1998), arXiv:hep-ph/9707481 [hep-ph].
- [27] Nora Brambilla, Antonio Pineda, Joan Soto, and Antonio Vairo, "Potential NRQCD: An effective theory for heavy quarkonium," Nucl. Phys. B 566, 275 (2000), arXiv:hep-ph/9907240 [hep-ph].
- [28] Nora Brambilla, Gastão Krein, Jaume Tarrús Castellà, and Antonio Vairo, "Long-range properties of 1S bottomonium states," Phys. Rev. D 93, 054002 (2016), arXiv:1510.05895 [hep-ph].
- [29] Stanley J. Brodsky, Ivan A. Schmidt, and Guy F. de Téramond, "Nuclear bound quarkonium," Phys. Rev. Lett. 64, 1011 (1990).
- [30] Alexei B. Kaidalov and Peter E. Volkovitsky, "Heavy quarkonia interactions with nucleons and nuclei," Phys. Rev. Lett. 69, 3155 (1992).
- [31] David A. Wasson, "Comment on 'Nuclear bound quarkonium'," Phys. Rev. Lett. 67, 2237 (1991).
- [32] Michael E. Luke, Aneesh V. Manohar, and Martin J. Savage, "A QCD calculation of the interaction of quarkonium with nuclei," Phys. Lett. B 288, 355 (1992), arXiv:hep-ph/9204219 [hep-ph].
- [33] Kazuo Yokokawa, Shoichi Sasaki, Tetsuo Hatsuda, and Arata Hayashigaki, "First lattice study of low-energy charmonium-hadron interaction," Phys. Rev. D 74, 034504 (2006), arXiv:hep-lat/0605009 [hep-lat].
- [34] Liuming Liu, Huey-Wen Lin, and Kostas Orginos, "Charmed Hadron Interactions," Proceedings, 26th International Symposium on Lattice field theory (Lattice 2008), PoS LATTICE2008, 112 (2008), arXiv:0810.5412 [hep-lat].

- [35] Silas R. Beane, Emmanuel Chang, Saul D. Cohen, William Detmold, Huey-Wen Lin, Kostas Orginos, Assumpta Parreño, and Martin J. Savage (NPLQCD Collaboration), "Quarkonium-nucleus bound states from Lattice QCD," Phys. Rev. D 91, 114503 (2015), arXiv:1410.7069 [hep-lat].
- [36] Taichi Kawanai and Shoichi Sasaki, "Charmoniumnucleon potential from Lattice QCD," Phys. Rev. D 82, 091501 (2010), arXiv:1009.3332 [hep-lat].
- [37] David G. Richards, Don K. Sinclair, and Dennis W. Sivers, "Lattice QCD simulation of meson exchange forces," Phys. Rev. D 42, 3191 (1990).
- [38] Petrus Pennanen, Christopher Michael, and Anthony M. Green (UKQCD Collaboration), "Interactions of heavy light mesons," Lattice field theory. Proceedings, 17th International Symposium, Lattice'99, Pisa, Italy, June 29-July 3, 1999, Nucl. Phys. Proc. Suppl. 83, 200 (2000), arXiv:hep-lat/9908032 [hep-lat].
- [39] Gunnar S. Bali, Hartmut Neff, Thomas Düssel, Thomas Lippert, and Klaus Schilling (SESAM Collaboration), "Observation of string breaking in QCD," Phys. Rev. D 71, 114513 (2005), arXiv:hep-lat/0505012 [hep-lat].
- [40] Gunnar Bali and Martin Hetzenegger (QCDSF Collaboration), "Static-light meson-meson potentials," Proceedings, 28th International Symposium on Lattice field theory (Lattice 2010), Proc. Science LATTICE2010, 142 (2010), arXiv:1011.0571 [hep-lat].
- [41] Antje Peters, Pedro Bicudo, Krzysztof Cichy, and Marc Wagner, "Investigation of BB four-quark systems using Lattice QCD," in 4th FAIR NExt generation ScientistS (FAIRNESS 2016) Garmisch-Partenkirchen, Germany, February 14-19, 2016 (2016) arXiv:1602.07621 [hep-lat].
- [42] Gunnar Bali and Martin Hetzenegger (QCDSF Collaboration), "Potentials between pairs of static-light mesons," Proceedings, 29th International Symposium on Lattice field theory (Lattice 2011), Proc. Science LATTICE2011, 123 (2011), arXiv:1111.2222 [hep-lat].
- [43] Keith A. Olive et al. (Particle Data Group), "Review of Particle Physics," Chin. Phys. C 38, 090001 (2014).
- [44] Mattia Bruno *et al.* (CLS), "Simulation of QCD with $N_f = 2 + 1$ flavors of non-perturbatively improved Wilson fermions," J. High Energy Phys. **02**, 043 (2015), arXiv:1411.3982 [hep-lat].
- [45] Martin Lüscher et al., http://luscher.web.cern.ch/luscher/openQCD/, accessed 2016.
- [46] Martin Lüscher and Stefan Schaefer, "Lattice QCD with open boundary conditions and twisted-mass reweighting," Comput. Phys. Commun. 184, 519 (2013), arXiv:1206.2809 [hep-lat].
- [47] Martin Lüscher, "Properties and uses of the Wilson flow in Lattice QCD," J. High Energy Phys. 08, 071 (2010), [Erratum: J. High Energy Phys. 03, 092 (2014)], arXiv:1006.4518 [hep-lat].
- [48] Gunnar S. Bali, Enno E. Scholz, Jakob Simeth, and Wolfgang Söldner (RQCD Collaboration), "Lattice simulations with $N_f = 2 + 1$ improved Wilson fermions at a fixed strange quark mass," Phys. Rev. D **94**, 074501 (2016), arXiv:1606.09039 [hep-lat].
- [49] Szabolcs Borsányi *et al.* (BMW-c), "High-precision scale setting in Lattice QCD," J. High Energy Phys. **09**, 010 (2012), arXiv:1203.4469 [hep-lat].
- [50] Björn Leder, https://github.com/bjoern-leder/wloop/, accessed 2016.

- [51] Michael Donnellan, Francesco Knechtli, Björn Leder, and Rainer Sommer (ALPHA Collaboration), "Determination of the static potential with dynamical fermions," Nucl. Phys. B 849, 45 (2011), arXiv:1012.3037 [hep-lat].
- [52] Anna Hasenfratz and Francesco Knechtli, "Flavor symmetry and the static potential with hypercubic blocking," Phys. Rev. D 64, 034504 (2001), arXiv:hep-lat/0103029 [hep-lat].
- [53] Michele Della Morte, Stephan Dürr, Jochen Heitger, Heiko Molke, Juri Rolf, Andrea Shindler, and Rainer Sommer (ALPHA Collaboration), "Lattice HQET with exponentially improved statistical precision," Phys. Lett. B 581, 93 (2004), [Erratum: Phys. Lett. B 612, 313 (2005)], arXiv:hep-lat/0307021 [hep-lat].
- [54] Anna Hasenfratz, Roland Hoffmann, and Francesco Knechtli, "The static potential with hypercubic blocking," Nucl. Phys. Proc. Suppl. 106, 418 (2002), arXiv:hep-lat/0110168 [hep-lat].
- [55] Michele Della Morte, Andrea Shindler, and Rainer Sommer (ALPHA Collaboration), "On lattice actions for static quarks," J. High Energy Phys. 08, 051 (2005), arXiv:hep-lat/0506008 [hep-lat].
- [56] Alois Grimbach, Damiano Guazzini, Francesco Knechtli, and Filippo Palombi (ALPHA Collaboration), "O(a) improvement of the HYP static axial and vector currents at one-loop order of perturbation theory," J. High Energy Phys. **03**, 039 (2008), arXiv:0802.0862 [hep-lat].
- [57] Ulli Wolff (ALPHA Collaboration), "Monte Carlo errors with less errors," Comput. Phys. Commun. 156, 143 (2004), arXiv:hep-lat/0306017 [hep-lat].
- [58] Stefan Schaefer, Rainer Sommer, and Francesco Virotta (ALPHA Collaboration), "Critical slowing down and error analysis in Lattice QCD simulations," Nucl. Phys. B 845, 93 (2011), arXiv:1009.5228 [hep-lat].
- [59] Silvia Necco and Rainer Sommer, "The N_f = 0 heavy quark potential from short to intermediate distances," Nucl. Phys. B 622, 328 (2002), arXiv:hep-lat/0108008.
- [60] Estia Eichten, Kurt Gottfried, Toichiro Kinoshita, John B. Kogut, Kenneth D. Lane, and Tung-Mow Yan, "The spectrum of charmonium," Phys. Rev. Lett. 34, 369 (1975), [Erratum: Phys. Rev. Lett. 36, 1276 (1976)].
- [61] Vanessa Koch, John Bulava, Ben Hörz, Francesco Knechtli, Graham Moir, Colin Morningstar, and Mike Peardon, "Towards string breaking with 2+1 dynamical fermions using the stochastic LapH method," Proceedings, 33rd International Symposium on Lattice Field Theory (Lattice 2015): Kobe, Japan, July 14-18, 2015, Proc. Science LATTICE2015, 100 (2016), arXiv:1511.04029 [hep-lat].
- [62] Rainer Sommer, "A new way to set the energy scale in lattice gauge theories and its applications to the static force and α_s in SU(2) Yang-Mills theory," Nucl. Phys. B **411**, 839 (1994), arXiv:hep-lat/9310022 [hep-lat].
- [63] Gunnar S. Bali and Peter Boyle, "A Lattice potential investigation of quark mass and volume dependence of the Υ spectrum," Phys. Rev. D 59, 114504 (1999), arXiv:hep-lat/9809180 [hep-lat].
- [64] Simon Kreuzer and Hans-Werner Hammer, "On the modification of the Efimov spectrum in a finite cubic box," Eur. Phys. J. A 43, 229 (2010), arXiv:0910.2191 [nucl-th].
- [65] Kathryn Polejaeva and Akaki Rusetsky, "Three particles in a finite volume," Eur. Phys. J. A48, 67 (2012), arXiv:1203.1241 [hep-lat].

- [66] Raúl A. Briceño and Zohreh Davoudi, "Three-particle scattering amplitudes from a finite volume formalism," Phys. Rev. D 87, 094507 (2013), arXiv:1212.3398 [heplat].
- [67] Ulf-G. Meißner, Guillermo Ríos, and Akaki Rusetsky, "Spectrum of three-body bound states in a finite volume," Phys. Rev. Lett. 114, 091602 (2015), [Erratum: Phys. Rev. Lett. 117, 069902 (2016)], arXiv:1412.4969 [hep-lat].
- [68] Maxwell T. Hansen and Stephen R. Sharpe, "Expressing the three-particle finite-volume spectrum in terms of the three-to-three scattering amplitude," Phys. Rev. D 92, 114509 (2015), arXiv:1504.04248 [hep-lat].
- [69] Maxwell T. Hansen and Stephen R. Sharpe, "Threshold expansion of the three-particle quantization condition," Phys. Rev. D 93, 096006 (2016), arXiv:1602.00324 [heplat].
- [70] Estia Eichten and Frank L. Feinberg, "Spin dependent forces in QCD," Phys. Rev. D 23, 2724 (1981).
- [71] Alberto Barchielli, Nora Brambilla, and Giovanni M. Prosperi, "Relativistic corrections to the quark-antiquark potential and the quarkonium spectrum," Nuovo Cim. A 103, 59 (1990).
- [72] Gunnar S. Bali, Klaus Schilling, and Armin Wachter, "Complete $O(v^2)$ corrections to the static interquark potential from SU(3) gauge theory," Phys. Rev. D **56**, 2566 (1997), arXiv:hep-lat/9703019 [hep-lat].
- [73] Gunnar S. Bali, "QCD forces and heavy quark bound states," Phys. Rept. 343, 1 (2001), arXiv:hepph/0001312 [hep-ph].
- [74] Nora Brambilla, Antonio Pineda, Joan Soto, and Antonio Vairo, "Effective field theories for heavy quarkonium," Rev. Mod. Phys. 77, 1423 (2005), arXiv:hep-ph/0410047 [hep-ph].
- [75] Yoshiaki Koma and Miho Koma, "Spin-dependent potentials from lattice QCD," Nucl. Phys. B 769, 79 (2007), arXiv:hep-lat/0609078 [hep-lat].

- [76] Francesco Knechtli, Maurizio Alberti, Gunnar S. Bali, Sara Collins, Graham Moir, and Wolfgang Söldner, "Testing the hadro-quarkonium model on the lattice," Proceedings, 34th International Symposium on Lattice Field Theory (Lattice 2016), Proc. Science LAT-TICE2016, 113 (2017), arXiv:1611.00912 [hep-lat].
- [77] Paul Arts et al., "QPACE 2 and domain decomposition on the Intel Xeon Phi," Proceedings, 32nd International Symposium on Lattice Field Theory (Lattice 2014), Proc. Science LATTICE2014, 021 (2015), arXiv:1502.04025 [cs.DC].
- [78] Robert G. Edwards and Balint Joó (SciDAC, LHP Collaboration and UKQCD Collaboration), "The Chroma software system for lattice QCD," Nucl. Phys. B Proc. Suppl. 140, 832 (2005), arXiv:hep-lat/0409003.
- [79] Simon Heybrock, Matthias Rottmann, Peter Georg, and Tilo Wettig, "Adaptive algebraic multigrid on SIMD architectures," Proceedings, 33rd International Symposium on Lattice Field Theory (Lattice 2015), Proc. Science LATTICE2015, 036 (2016), arXiv:1512.04506 [physics.comp-ph].
- [80] Daniel Richtmann, Simon Heybrock, and Tilo Wettig, "Multiple right-hand-side setup for the DD-αAMG," Proceedings, 33rd International Symposium on Lattice Field Theory (Lattice 2015), Proc. Science LATTICE2015, 035 (2016), arXiv:1601.03184 [hep-lat].
- [81] Simon Heybrock, Bálint Joó, Dhiraj D. Kalamkar, Mikhail Smelyanskiy, Karthikeyan Vaidyanathan, Tilo Wettig, and Pradeep Dubey, "Lattice QCD with domain decomposition on Intel Xeon Phi co-processors," The International Conference for High Performance Computing, Networking, Storage, and Analysis, New Orleans, LA, USA, November 16-21, 2014, Proceedings of SC14, 69 (2014), arXiv:1412.2629 [hep-lat].
- [82] Andreas Frommer, Karsten Kahl, Stefan Krieg, Björn Leder, and Matthias Rottmann, "Adaptive aggregation based domain decomposition Multigrid for the lattice Wilson Dirac operator," SIAM J. Sci. Comput. 36, A1581 (2014), arXiv:1303.1377 [hep-lat].